HSI-DETR: A DETR-based Transfer Learning from RGB to Hyperspectral Images for Object Detection of Live and Dead Cells

To achieve better results, convert models with the fewest changes from RGB to HSI.

Songxin Ye
College of Computer Science and Software Engineering, Shenzhen University, China
yesongxin2021@email.szu.edu.cn

Nanying Li
College of Computer Science and Software Engineering, Shenzhen University, China
linanying2021@email.szu.edu.cn

Jiaqi Xue
College of Computer Science and Software Engineering, Shenzhen University, China
xuejiaqi2021@email.szu.edu.cn

Yaqian Long
College of Computer Science and Software Engineering, Shenzhen University, China
longyaqian@szu.edu.cn

Sen Jia*
College of Computer Science and Software Engineering, Shenzhen University, China;
senjia@szu.edu.cn

ABSTRACT

Traditional cell viability judgment methods are invasive and damaging to cells. Moreover, even under a microscope, it is difficult to distinguish live cells from dead cells by the naked eye alone. With the development of optical imaging technology, hyperspectral imaging is more and more widely used in various fields. Hyperspectral imaging is a non-contact optical technique that provides both spectral and spatial information in a single measurement. It becomes a fast, non-invasive option to differentiate between live and dead cells. In recent years, the rapid development of deep learning has provided a better way to distinguish the difference between living and dead cells through a large amount of data. However, it is often necessary to acquire large amounts of labeled data at an expensive cost to train models. This is more difficult to achieve on medical hyperspectral images. Therefore, in this paper, a new model called HSI-DETR is proposed to solve the above problem on the target detection task of live and dead cells, which is based on the detection transformer (DETR) model. The HSI-DETR model suitable for hyperspectral images (HSI) is proposed with minimal modification. Then, some parameters of DETR trained on RGB images are transferred to HSI-DETR trained on hyperspectral images. Compared to the general method, this method can train a better model with a small number of labeled samples. And compared to the DETR-R50, the AP50 of HSI-DETR-R50 has increased by 5.15%.

*Corresponding author

ICCPR 2022, November 17–19, 2022, Beijing, China

ACM ISBN 978-1-4503-9705-6/22/11…$15.00
https://doi.org/10.1145/3581807.3581822

CCS CONCEPTS

• **Computing methodologies**; • **Artificial intelligence**; • **Life and medical sciences**;

KEYWORDS

object detection, hyperspectral imaging, live and dead cells, HSI-DETR

ACM Reference Format:
Songxin Ye, Nanying Li, Jiaqi Xue, Yaqian Long, and Sen Jia. 2022. HSI-DETR: A DETR-based Transfer Learning from RGB to Hyperspectral Images for Object Detection of Live and Dead Cells: To achieve better results, convert models with the fewest changes from RGB to HSI.. In *2022 11th International Conference on Computing and Pattern Recognition (ICCPR) (ICCPR 2022), November 17–19, 2022, Beijing, China.* ACM, New York, NY, USA, 6 pages. https://doi.org/10.1145/3581807.3581822

1 INTRODUCTION

Cell viability is an important indicator for judging whether cells cultured in vitro can grow normally under certain conditions, such as drug treatment, radioactive or ultraviolet irradiation, and changes in culture conditions. It is a common method for scientific research in related fields, and it is also one of the important methods for in vitro screening of antitumor drugs and clinical tumor drug susceptibility tests. At present, there are many methods commonly used to detect cell viability, such as the staining counting method represented by trypan blue staining and fluorescent staining [1, 2], the colony formation test is used to determine the proliferation ability of single cells to distinguish cell viability [3, 4], colorimetric methods represented by SRB method, AlanlarBlue method, and ATP content determination method, and instrumental analysis methods including liquid scintillation counter method and flow cytometry (FCM) method [2]. These existing methods for judging cell viability are more or less likely to damage the cells, resulting in significant changes in the appearance or characteristics of the cells, tedious operations, and high time costs. Moreover, it notes that cell death is often associated with morphological changes such as cell membrane blistering, organelle expansion, and nucleus enrichment [7, 8]. In addition, dead cells have lower forward scattering and higher

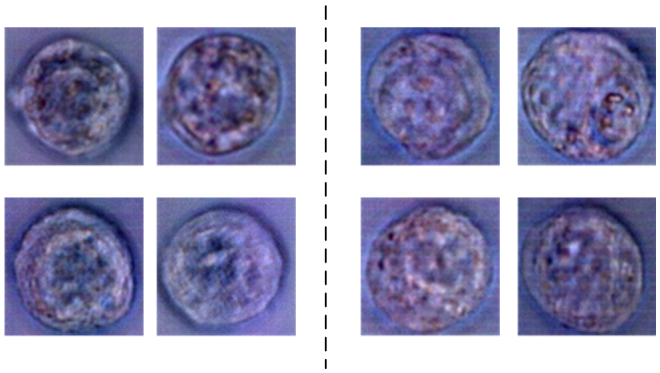

Figure 1: RGB images of dead cells (left) and live cells (right).

lateral scattering compared to live cells [9]. However, even with the help of a microscope or flow cytometer, these subtle changes are difficult to discern with the naked eye (see Figure 1 for examples).

Hyperspectral imaging is an advanced technology for capturing image spatial information and spectral information [5], which is developed based on multispectral remote sensing technology. This method has the advantage of being convenient and non-invasive when acquiring hyperspectral images of cells. It integrates two traditional optical diagnostic methods of spectral analysis and optical imaging, with high spectral resolution and spatial resolution. Therefore, it can provide 2-dimensional spatial information and 1-dimensional spectral information of the imaging object at the same time, thereby reflecting its chemical composition information and physical form information. This technology was originally used for aerial remote sensing, such as environmental detection and military reconnaissance. Later, it gradually expanded from the military field to commercial applications. In recent years, thanks to the rapid development of artificial intelligence technology and precision medicine theory, hyperspectral imaging technology has shown great application potential in the field of biomedicine [6].

Chen et al. [10] built a cell imaging system with a microscope and a hyperspectral camera to collect hyperspectral images of primitive cells. They then used support vector machine classification methods on these data to prove that HSI is better than RGB images in extracting features that distinguish live cells from dead cells. This means that more spectral information helps distinguish live cells from dead cells. Notably, this method is not invasive to cells compared to traditional methods of distinguishing cell activity. This points out a way for us to explore the differentiation of cell activity through hyperspectral images, and how to distinguish fine changes between live and dead cells through spatial structure and spectral morphological features has become a worthy research direction.

The following three practical issues are considered. The first point is that in real applications, rather than distinguishing between live cells and dead cells, the more valuable requirement is to count the respective numbers of live cells and dead cells to calculate the survival of cells rate and locate live and dead cells separately in the scene to separate them. Therefore, the target detection task of live and dead cells is more valuable. Second, in the field of medical imaging, especially in the field of hyperspectral medical imaging, the difficulty of data collection and the high cost of labeling make it impossible to obtain a large amount of labeling data. Therefore, how to obtain better results with fewer data has become our research direction, that is, the study of small sample learning. Last but not least, considering the morphological indistinguishability of live cells and dead cells, as well as the specific differences in spectra, HSI data are introduced for the study. In this paper, a small sample-based hyperspectral images detection transformer (HSI-DETR) capable of extracting more spectral information for the detection of live and dead cells is proposed.

2 RELATED WORK

2.1 Medical hyperspectral imaging

Hyperspectral microscopy imaging systems are mainly composed of imaging spectrometers, CCD (charge-coupled device) cameras, and microscopes [11]. If classified according to the data acquisition method, hyperspectral microscopy imaging systems are mainly divided into scanning type and snapshot type. Among them, the scanning hyperspectral imaging system can be subdivided into whiskbroom, pushbroom and staring [6]. Hu et al. [12] (2019) established a hyperspectral database of 30 gastric cancer patients using hyperspectral microscopy technology. Based on the difference in spectral-spatial characteristics between gastric cancer tissue and normal tissue in the wavelength range of 410~910 nm, they proposed a deep learning-based analysis method for gastric cancer tissue. Leon et al. [13] (2020) proposed an HSI-based dermatological acquisition system, which captured 125 spectral bands in the 450–950 nm spectral range and obtained 76 pigmented skin lesions from 61 patients, and used them to detect whether the lesions were benign or malignant. Chen et al. [10] (2019) proposed a cell imaging system consisting of microscopy, hyperspectral camera-based hardware and related software system components for capturing original HSI images. They used this system to collect hyperspectral imaging data of human ovarian cancer cells that are widely used in tumor-related research. And they used these data to set up relevant experiments to demonstrate that hyperspectral images (HSI) are more useful than RGB images in distinguishing between live and dead cells. The data of the experiments in this paper are obtained after processing based on the data collected by them.

2.2 ICA-based Band Selection

Although HSI can provide rich information about objects, their high dimensionality also greatly increases the computational burden and is prone to dimensional disaster. To solve this problem, dimensionality reduction has become our choice. Dimensionality reduction is a commonly used method for HSI analysis. Through dimensionality reduction, redundant information can be removed and the operation efficiency can be improved. At present, the methods of dimensionality reduction are mainly based on band selection and feature extraction. Band selection is to remove some bands by some specific methods, and retain some bands of HSI data. Feature extraction is to transform the original hyperspectral data into a new feature space by transforming the original HSI.

In this paper, a band selection method based on independent component analysis (ICA) proposed by Du et al. [14] is used, which observes the contribution of each band to the ICA decomposition

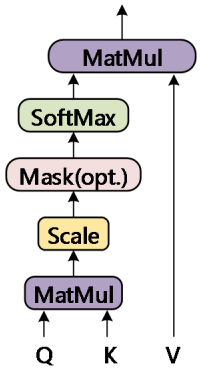

Figure 2: The structure of Self-attention

process by evaluating the weight matrix, and after comparing the mean absolute weight coefficients of each spectral band, selects the band that contains more information. The band selection method based on ICA has a significant advantage in preserving most of the physical characteristics of the spectral profile.

2.3 End-to-end object detection algorithm: DETR

Transformer [15] has been widely used in the field of computer vision since it was proposed in 2017. And many remarkable achievements have been made in these fields, even surpassing convolution neural networks in many works. Detection transformer (DETR) [16] is a typical representative of these works [19], which successfully applies transformers to object detection. It effectively eliminates the need for the manual design of many hand-designed components such as non-maxima suppression and anchor generation. The model in this paper is based on DETR, with minimal modifications, making it suitable for HSI target detection tasks to achieve better results.

The heart of the Transformer is self-attention (SA), which consists of an encoder and a decoder with several transformer blocks of the same architecture. Each transformer block is composed of a multi-head attention layer, a feed-forward neural network, shortcut connection and layer normalization. The success of transformers, to a great extent, depends on the use of multi-head attention, where multiple SA layers are stacked and integrated. Figure 2 illustrates the process of the SA module in transformers. In the self-attention layer, the input vector is first transformed into three different vectors: the query vector q, the key vector k and the value vector v. It is worth noting that they have the same dimensions. Vectors derived from different inputs are then packed together into three different matrices, named **Q**, **K** and **V**. Subsequently, the attention function is defined as formula (1) [17].

$$\text{Attention}(\mathbf{Q}, \mathbf{K}, \mathbf{V}) = \text{softmax}\left(\frac{\mathbf{Q} \cdot \mathbf{K}^{\mathrm{T}}}{\sqrt{d_k}}\right) \cdot \mathbf{V} \tag{1}$$

where **Q**, **K** and **V** are different matrices packed from different inputs, d_k is the dimension of query and key.

2.4 Data processing

The raw HSI data are collected by Chen et al. [10], which consisted of containing only live cells, containing only dead cells, and blank background images without cells (as shown in the background sample in Figure 3). The locations of individual live and dead cells in collected HSI are annotated, and then they are cropped to obtain single-cell data, as shown in Figure 1. In addition, due to the limited amount of data obtained by cropping, the data is expanded by rotating and flipping to expand the number of single cells to 8 times the original.

As mentioned in the introduction, live and dead cells are indistinguishable to the naked eye, and there is no good way to label mixed samples of live and dead cells, so we artificially generated labeled mixed samples. Randomly generate single live or dead cells on a background image, then generate location and class labels for new data based on where they were generated and the width and height of the cells. The resulting data sample is shown in Figure 4.

In addition, to make the training model more stable and accelerate the convergence of the network model, 50 original samples are randomly selected to calculate the mean and standard deviation of each band, and then normalized all the data through formula (2). That needs to be improved, and corresponding improvements will be proposed later.

$$\mathrm{X}_{\text{scale}} = \frac{\mathbf{x} - \mu}{\mathrm{S}} \tag{2}$$

where **X** is the raw data, μ is the mean, **S** is the standard deviation, and **X**scale is the normalized data.

2.5 HSI-DETR

The structure of HIS-DETR is shown in Figure 4, after testing, it is found that when all the data is directly put into the model training, the speed is very slow . There is a common dimensional disaster. Therefore, ICA-based Band Selection is used to select the original 150 bands data to obtain 10 bands data. This small step is of great help to improve our operation speed.

The new data is extracted features through a layer of HSI-Resnet that is simply modified by Resnet for HIS, then it passes through the same Transformer encoder and decoder as DETR. Finally, obtain the predicted target box and category information by the MLP prediction head. The core structure of DETR is shown in Figure 5, which simplifies the detection pipeline by discarding multiple hand-designed components that encode prior knowledge, such as spatial anchors and non-maximum suppression.

It uses the classic convolution network as the backbone network, then puts its extracted feature set into a pair of Transformer encoders and decoders, and finally uses Multi-Layer Perception (MLP) as the prediction header of the network to output the target box and category information. It is worth noting that DETR predicts a total of N bounding boxes. N is a preset value that is much larger than the number of targets in the picture. The ground truth that exceeds the number of targets uses the background element as a negative sample.

As for the changes to HSI-Resnet, as shown in Figure 6, the changes made are so simple. The number of input channels of the first convolution layer of Resnet is changed from the original 3 to 10, and a Batch Normalization layer is added before it, which is

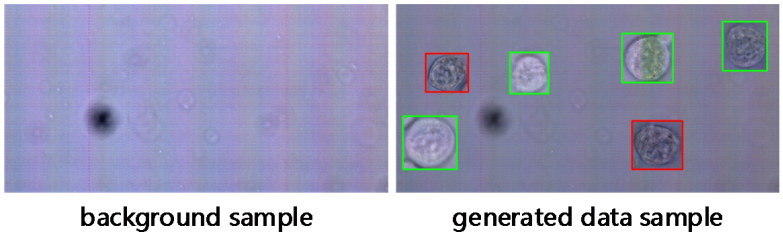

Figure 3: The sample of background and generated data

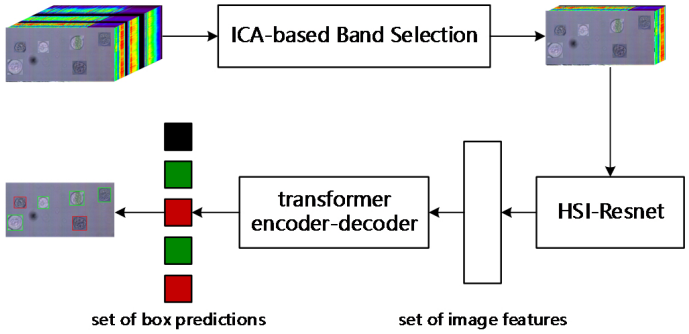

Figure 4: The structure of HIS-DETR

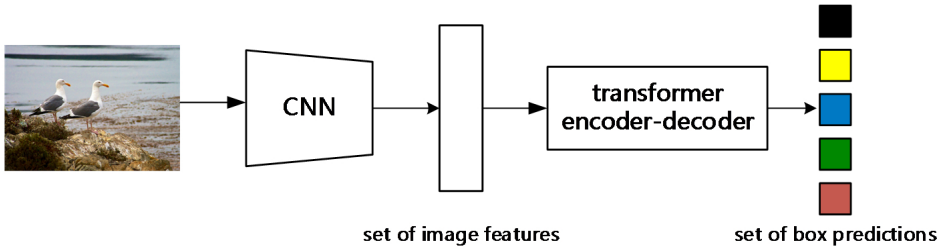

Figure 5: The structure of DETR

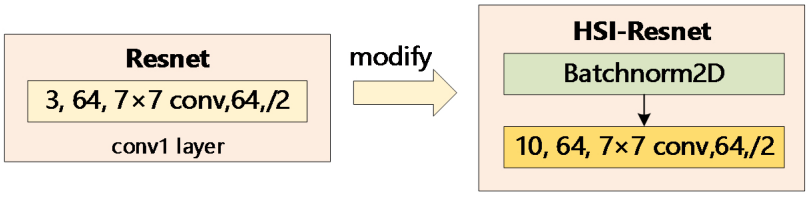

Figure 6: The changes from Resnet to HSI-Resnet

intended to eliminate the error effect of only considering part of the sample when normalizing the data. The motivation for doing so is to make the smallest changes in exchange for the greatest gains, which have proven to be useful.

2.6 Loss function

Another important work of DETR is the design of the loss function. As mentioned earlier, DETR will predict a total of N bounding boxes, and this N is a preset value that is much larger than the number of targets in the picture. Except for the target to be predicted, the others are background classes. The background class accounts for the vast majority of all predicted bounding boxes. When calculating the loss, DETR's strategy is to fill the ground truth by increasing the background classes without target objects, so that the number of ground truth is consistent with the number of predicted bounding boxes. The matching cost of ground truth $\boldsymbol{y}_i$ and a prediction with index $\sigma(i)$ is defined as shown in the formula (3). After defining the matching cost, the Hungarian matching algorithm is used to obtain

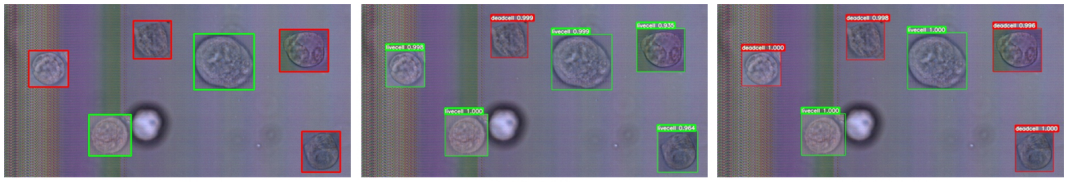

Figure 7: Comparison of the results of different methods (dead cells are green and live cells are red)

the optimal binary matching scheme of the ground truth and the bounding box. Finally, the loss function can be defined as formula (4).

$$\mathcal{L}_{\text{match}}\left(\boldsymbol{y}_i, \hat{\boldsymbol{y}}_{\sigma(i)}\right) = -1_{\{c_i \neq \emptyset\}} \hat{\boldsymbol{p}}_{\sigma(i)}\left(c_i\right) + 1_{\{c_i \neq \emptyset\}} \mathcal{L}_{\text{box}}\left(\boldsymbol{b}_i, \hat{\boldsymbol{b}}_{\sigma(i)}\right) \tag{3}$$

where $1_{\{c_i \neq \emptyset\}}$ is a bool function that is 1 when $c_i \neq \emptyset$, 0 otherwise. c_i is the category label for the ith object. $\sigma(i)$ is the index of the bounding box that matches the ith target. $\hat{\boldsymbol{p}}_{\sigma(i)}(\boldsymbol{c_i})$ represents the probability that the category of the $\sigma(i)$ predicted by DETR is c_i. $\boldsymbol{b_i}$ and $\hat{\boldsymbol{b}}_{\sigma(i)}$ are the coordinates of the ground truth (center point, width, height) of the position of the ith target and the coordinates of the predicted bounding box, respectively.

$$\hat{\sigma} = \underset{\sigma \in G_N}{\arg min} \sum_{i}^{N} \mathcal{L}_{\text{match}}\left(\boldsymbol{y}_i, \hat{\boldsymbol{y}}_{\sigma(i)}\right) \tag{4}$$

2.7 Transfer parameters

It is found that if the parameters of the model are directly initialized randomly, the HSI-DETR could not learn useful information. Therefore, when initializing the model parameters, in addition to the modified layer, the parameters learned by DETR on the coco dataset are transferred to HSI-DETR. The reason for this will be mentioned next. This step seems simple, but it plays a crucial role in the convergence of the model.

3 EXPERIMENT

3.1 Dataset and experiment details

A total of 6418 HSI were generated, each containing 1 to 8 cell instances. Considering the high cost of obtaining high-quality labeled medical image data in reality, it is sought to obtain better results with less training data. Therefore, only 5% of data are selected as training samples in this experiment, and the remaining 95% as test data, with a total of 320 images in the training set and 6098 images in the test set. The batch size is set to 8 and the epoch is set to 500.

The HSI-DETR is trained with AdamW [18] setting the initial transformer's learning rate to 10^{-4}, the backbone's learning rate to 10^{-5}, and weight decay to 10^{-4}. All unmodified network layers will be initialized with the weights that DETR trained on the coco dataset. The width of the input image is set to 640 and the height is set to 320.

3.2 Experimental analysis

The principal component analysis method (PCA) [19] is used to reduce the dimensionality of the HSI data, and then the data is entered into the model for training. The interesting phenomenon is found that if we initialize the parameters of the model like DETR and train the model directly, the model can hardly learn anything. After analysis, the reason is attributed to the insufficient amount of data. So the weights trained by DETR on the coco dataset is used as the initialization weights of the model. The model is indeed converged, and some knowledge has been learned.

When training HSI-DETR, the same problem as above appeared. So a bold idea is born, of whether the parameters of the network layer that have not changed can also be transferred from the weights learned from the coco dataset. It turns out that this approach is simple and effective. We report results with two different backbones: a ResNet-50 and a ResNet-101. As shown in Table 1, although our method looks simple, its AP50 improvement proves its effectiveness. As can be seen from Table 1, the AP50 of HSI-DETR-R50 is 5.87% higher than that of DETR-R50, and the AP50 of HSI-DETR-R101 is 5.15% higher than that of DETR-R101. As can be seen from Figure 7, our method has a better detection effect and higher accuracy than the comparison method. The experiments not only provide a new idea for models trained on traditional RGB images to migrate to HSI, but also proves once again that more spectral information is very helpful in distinguishing differential characteristics in the identification of live and dead cells.

In the Methods section, it is mentioned that when normalizing the data, a portion of the sample is randomly drawn to calculate the mean and standard deviation to normalize the data. After realizing that there is room for improvement in this approach, a Batch Normalization layer was added to the first layer of the network to try to eliminate this effect. From the results of the ablation experiments in Table 2, it can be seen that this improvement greatly contributes to the improvement of the model.

4 CONCLUSION

Based on previous research work on the distinction between live and dead cells, this paper raises a new question, target detection of live and dead cells in mixed cells. At the same time, the improved HIS-DETR based on the DETR model is proposed, which verifies the effectiveness of this idea by achieving better migration effects with the least modification. In addition, by extracting the subtle differences in spectral information between live and dead cells, the separability and discrimination of live and dead cells can be more effectively improved, so that the recognition effect can be effectively improved even under the condition of small samples. How to further explore more spectral information features, in the case of fewer samples, is worthwhile to achieve better identification results Direction of the research.

Table 1: Results of the comparison of different methods

Model	PCA	ICA-based Band Selection	AP_{50} (%)
Yolov5	✓		66.67
DETR-R50	✓		67.08
HSI-DETR-R50		✓	**72.95**
DETR-R101	✓		68.34
HSI-DETR-R101		✓	**73.49**

Table 2: Results of ablation experiments with Batch Normalization layer

Model	Batch Normalization layer	AP_{50} (%)
HSI-DETR-R50		70.04
HSI-DETR-R50	✓	**72.95**
HSI-DETR-R101		72.32
HSI-DETR-R101	✓	**73.49**

ACKNOWLEDGMENTS

The work is supported by the National Natural Science Foundation of China (Grant No. 62271327, 41971300), the Key Project of Department of Education of Guangdong Province (Grant No. 2020ZDZX3045), the Guangdong Basic and Applied Basic Research Foundation (Grant No. 2022A1515011290), Shenzhen Science and Technology Program (Grant No. KQTD20200909113951005).

REFERENCES

[1] Xinjian Yang. 2013. Animal cell culture. China Agricultural University Press.
[2] Zhennan Situ and Junzheng Wu. 2007. Cell culture. World Book Publishing.
[3] Dorota Banasiak, Anthony R. Barnetson, Ross A. Odell, Hedy Mameghan, and Pamela J. Russell. 1999. Comparison between the clonogenic, MTT, and SRB assays for determining radiosensitivity in a panel of human bladder cancer cell lines and a ureteral cell line. Radiation Oncology Investigations 7, 2: 77–85. https://doi.org/10.1002/(SICI)1520-6823(1999)7:2<77::AID-ROI3>3.0.CO;2-M
[4] Bea Pauwels, Annelies E. C. Korst, Christel M. J. de Pooter, Greet G. O. Pattyn, Hilde A. J. Lambrechts, Marc F. D. Baay, Filip Lardon, and Jan B. Vermorken. 2003. Comparison of the sulforhodamine B assay and the clonogenic assay for in vitro chemoradiation studies. Cancer Chemotherapy and Pharmacology 51, 3: 221–226. https://doi.org/10.1007/s00280-002-0557-9
[5] Junshi Xia, Nicola Falco, Jón Atli Benediktsson, Peijun Du, and Jocelyn Chanussot. 2017. Hyperspectral Image Classification With Rotation Random Forest Via KPCA. IEEE Journal of Selected Topics in Applied Earth Observations and Remote Sensing 10, 4: 1601–1609. https://doi.org/10.1109/JSTARS.2016.2636877
[6] Guolan Lu and Baowei Fei. 2014. Medical hyperspectral imaging: a review. Journal of Biomedical Optics 19, 1: 010901. https://doi.org/10.1117/1.JBO.19.1.010901
[7] S. Rello, J. C. Stockert, V. Moreno, A. Gámez, M. Pacheco, A. Juarranz, M. Cañete, and A. Villanueva. 2005. Morphological criteria to distinguish cell death induced by apoptotic and necrotic treatments. Apoptosis 10, 1: 201–208. https://doi.org/10.1007/s10495-005-6075-6
[8] In Vitro Morphological Assessment of Apoptosis Induced by Antiproliferative Constituents from the Rhizomes of Curcuma zedoaria. Retrieved August 24, 2022 from https://www.hindawi.com/journals/ecam/2013/257108/
[9] Z Darzynkiewicz and E Bedner. 2000. Analysis of apoptotic cells by flow and laser scanning cytometry. Methods in enzymology 322: 18–39. https://doi.org/10.1016/s0076-6879(00)22005-3
[10] He Chen, Benjamin Ho, Haofei Wang, Say Hwa Tan, Chun-Xia Zhao, Nam-Trung Nguyen, Yongsheng Gao, and Jun Zhou. 2019. Automatic Live and Dead Cell Classification via Hyperspectral Imaging. In 2019 10th Workshop on Hyperspectral Imaging and Signal Processing: Evolution in Remote Sensing (WHISPERS), 1–5. https://doi.org/10.1109/WHISPERS.2019.8921136
[11] K Ajay Kumar, Nitesh Thapa, and Saji A Kuriakose. 2015. Advances in spaceborne hyperspectral imaging systems. HYPERSPECTRAL REMOTE SENSING 108, 5: 7.
[12] Bingliang Hu, Bingliang Hu, Jian Du, Jian Du, Zhoufeng Zhang, Zhoufeng Zhang, Quan Wang, and Quan Wang. 2019. Tumor tissue classification based on micro-hyperspectral technology and deep learning. Biomedical Optics Express 10, 12: 6370–6389. https://doi.org/10.1364/BOE.10.006370
[13] Raquel Leon, Beatriz Martinez-Vega, Himar Fabelo, Samuel Ortega, Veronica Melian, Irene Castaño, Gregorio Carretero, Pablo Almeida, Aday Garcia, Eduardo Quevedo, Javier A. Hernandez, Bernardino Clavo, and Gustavo M. Callico. 2020. Non-Invasive Skin Cancer Diagnosis Using Hyperspectral Imaging for In-Situ Clinical Support. Journal of Clinical Medicine 9, 6: 1662. https://doi.org/10.3390/jcm9061662
[14] Hongtao Du, Hairong Qi, Xiaoling Wang, R. Ramanath, and W.E. Snyder. 2003. Band selection using independent component analysis for hyperspectral image processing. In 32nd Applied Imagery Pattern Recognition Workshop, 2003. Proceedings., 93–98. https://doi.org/10.1109/AIPR.2003.1284255
[15] Ashish Vaswani, Noam Shazeer, Niki Parmar, Jakob Uszkoreit, Llion Jones, Aidan N Gomez, Łukasz Kaiser, and Illia Polosukhin. 2017. Attention is All you Need. In Advances in Neural Information Processing Systems. Retrieved August 25, 2022 from https://proceedings.neurips.cc/paper/2017/hash/3f5ee243547dee91fbd053c1c4a845aa-Abstract.html
[16] End-to-End Object Detection with Transformers | SpringerLink. Retrieved August 25, 2022 from https://link.springer.com/chapter/10.1007/978-3-030-58452-8_13
[17] Kai Han, Yunhe Wang, Hanting Chen, Xinghao Chen, Jianyuan Guo, Zhenhua Liu, Yehui Tang, An Xiao, Chunjing Xu, Yixing Xu, Zhaohui Yang, Yiman Zhang, and Dacheng Tao. 2022. A Survey on Vision Transformer. IEEE Transactions on Pattern Analysis and Machine Intelligence: 1–1. https://doi.org/10.1109/TPAMI.2022.3152247
[18] Ilya Loshchilov and Frank Hutter. 2019. Decoupled Weight Decay Regularization. Retrieved August 30, 2022 from http://arxiv.org/abs/1711.05101
[19] Tarek El-Ghazawi, Sinthop Kaewpijit, and Jacqueline Le Moigne. 2001. Parallel and Adaptive Reduction of Hyperspectral Data to Intrinsic Dimensionality. 102–102. https://doi.org/10.1109/CLUSTR.2001.959958A